

## The Distribution of Earth-Impacting Interstellar Objects

DARRYL Z. SELIGMAN ,<sup>1,\*</sup> DUŠAN MARČETA ,<sup>2</sup> AND ELOY PEÑA-ASENSIO ,<sup>3,4</sup>

<sup>1</sup>*Dept. of Physics and Astronomy, Michigan State University, East Lansing, MI 48824, USA*

<sup>2</sup>*Department of Astronomy, Faculty of Mathematics, University of Belgrade, Studentski trg 16, Belgrade, 11000, Serbia*

<sup>3</sup>*Department of Aerospace Science and Technology, Politecnico di Milano, Via La Masa 34, 20156 Milano, Italy*

<sup>4</sup>*Department of Applied Mathematics and Aerospace Engineering, Universitat d'Alacant, 03690 Alacant, Spain*

### ABSTRACT

In this paper we calculate the expected orbital elements, radiants, and velocities of Earth-impacting interstellar objects. We generate a synthetic population of  $\sim 10^{10}$  interstellar objects with M-star kinematics in order to obtain  $\sim 10^4$  Earth-impactors. The relative flux of impactors arriving from the direction of the solar apex and the galactic plane is enhanced by a factor of  $\sim 2$  relative to the mean. The fastest impactors also arrive from these directions, although Earth-impactors are generally *slower* than objects in the overall population. This is because the Earth-impacting subset contains a higher fraction of low-eccentricity hyperbolic objects which are more strongly affected by gravitational focusing. Earth-impacting interstellar objects are more likely to have retrograde orbits close to the ecliptic plane. A selection effect makes the distribution of inclination of Earth-impacting interstellar objects uniform/sinusoidal at low/high perihelion distances. In turn, low perihelion impactors have higher impact probability towards the ecliptic plane. The overall impactor population therefore exhibits an intermediate inclination distribution between uniform and sinusoidal. The highest velocity impacts are most likely to occur in the spring when the Earth is moving towards the solar apex. However, impacts in general are more likely to occur during the winter when the Earth is located in the direction of the antapex. Interstellar objects are more likely to impact the Earth at low latitudes close to the equator, with a slight preference for the Northern hemisphere due to the location of the apex. These distributions are independent of the assumed interstellar object number density, albedos, and size-frequency distribution and are publicly available.

*Keywords:* Asteroids (72) — Comets (280) — Meteors (1041)

### 1. INTRODUCTION

The discovery of 1I/‘Oumuamua (G. V. Williams et al. 2017), 2I/Borisov (G. Borisov et al. 2019), and 3I/ATLAS (L. Denneau et al. 2025) demonstrated that large scale interstellar objects traverse the Solar System somewhat routinely. The number density of interstellar objects was estimated based on nondetections prior to the discovery of these two objects (Z. Sekanina 1976; T. A. McGlynn & R. D. Chapman 1989; P. J. Francis 2005; A. Moro-Martín et al. 2009; T. Engelhardt et al. 2017a). The discovery of 1I/‘Oumuamua implies a spatial number density of  $\sim 0.1 \text{ au}^{-3}$  (D. Jewitt et al. 2017; D. E. Trilling et al. 2017; G. Laughlin & K. Batygin 2017; A. Do et al. 2018; W. G. Levine et al. 2021) for

$\sim 100 \text{ m}$  scale interstellar objects. However, the precise value is extremely uncertain and the size-frequency distribution of the population is entirely unconstrained.

The three known interstellar objects exhibited divergent properties which are briefly summarized here. 1I/‘Oumuamua was photometrically inactive (K. J. Meech et al. 2017; Q.-Z. Ye et al. 2017; D. Jewitt et al. 2017; D. E. Trilling et al. 2018), although it had comet-like nongravitational acceleration (M. Micheli et al. 2018). While the high magnitude of nongravitational acceleration combined with lack of apparent comae was atypical, a population of near-Earth objects with similar properties have been reported (D. Farnocchia et al. 2023; D. Z. Seligman et al. 2023, 2024). 1I/‘Oumuamua had an extreme 6 : 6 : 1 geometry inferred from its light curve (M. Drahus et al. 2017; M. M. Knight et al. 2017; W. C. Fraser et al. 2018; A. McNeill et al. 2018; M. J. S. Belton et al. 2018; S. Mashchenko 2019) and a moder-

Email: dzs@msu.edu

\* NSF Astronomy and Astrophysics Postdoctoral Fellow

ately reddened reflection spectrum (J. Masiero 2017; A. Fitzsimmons et al. 2018; M. T. Bannister et al. 2017). 2I/Borisov was discovered in 2019 and displayed a dusty coma (D. Jewitt & J. Luu 2019; A. Fitzsimmons et al. 2019; Q. Ye et al. 2020; A. J. McKay et al. 2020; P. Guzik et al. 2020; M.-T. Hui et al. 2020; Y. Kim et al. 2020; G. Cremonese et al. 2020; B. Yang et al. 2021) with typical carbon- and nitrogen-bearing species (C. Opitom et al. 2019; T. Karetta et al. 2020; H. W. Lin et al. 2020; M. T. Bannister et al. 2020; Z. Xing et al. 2020; K. Aravind et al. 2021) and an enrichment of CO relative to H<sub>2</sub>O (D. Bodewits et al. 2020; M. A. Cordiner et al. 2020). 1I/‘Oumuamua and 2I/Borisov had nuclear radii of  $r_n \sim 80$  m and  $r_n \sim 400$  m respectively (D. Jewitt et al. 2020)<sup>5</sup>. 1I/‘Oumuamua, 2I/Borisov, and 3I/ATLAS had hyperbolic excess velocities of  $V_\infty \sim 26$  km s<sup>-1</sup>,  $V_\infty \sim 32$  km s<sup>-1</sup>, and  $V_\infty \sim 58$  km s<sup>-1</sup> corresponding to dynamical ages of  $\sim 10^2$ ,  $\sim 10^3$  Myr, and  $\sim 10$  Gyr (E. Mamajek 2017; E. Gaidos et al. 2017; F. Feng & H. R. A. Jones 2018; F. Almeida-Fernandes & H. J. Rocha-Pinto 2018; T. Hallatt & P. Wiegert 2020; C.-H. Hsieh et al. 2021; A. G. Taylor & D. Z. Seligman 2025; M. J. Hopkins et al. 2025b). 3I/ATLAS exhibited faint cometary activity and a reddened reflectance spectra similar to 1I/‘Oumuamua ad 2I/Borisov (D. Z. Seligman et al. 2025; C. Opitom et al. 2025; D. Jewitt & J. Luu 2025; M. R. Alarcon et al. 2025; R. de la Fuente Marcos et al. 2025; T. Karetta et al. 2025; C. O. Chandler et al. 2025; T. T. Frincke et al. 2025). We refer the reader to D. Jewitt & D. Z. Seligman (2023), A. Fitzsimmons et al. (2023), D. Z. Seligman & A. Moro-Martín (2023), and A. Moro-Martín (2022) for reviews on the topic of interstellar objects

In theory, a subset of these interstellar objects traversing the inner Solar System should impact the Earth. However, only  $\sim 1 - 10$  total  $\sim 100$  m scale interstellar objects should have impacted the Earth since it formed (D. Jewitt & D. Z. Seligman 2023). Moreover, distinguishing interstellar impact craters from solar system impact craters morphologically would be challenging (S. H. C. Cabot & G. Laughlin 2022). These interstellar-originating craters may be easier to identify on the lunar surface and potentially distinguishable based on their small radii, low latitudes, and high melt fractions (D. Chang et al. 2023).

Smaller scale interstellar objects have been identified throughout the Solar System. For example, presolar grains in meteorites provide examples of small solids

formed in extrasolar systems (E. Zinner 2014). Interstellar dust particles have been detected in-situ by both the Ulysses and the Galileo spacecraft, implying a Solar System flux of  $\sim 10^{-3} - 10^{-4}$  m<sup>-2</sup> s<sup>-1</sup> particles with  $10^{-7} - 10^{-6}$  m sizes (E. Grün et al. 1993; E. Grün et al. 1997; M. Landgraf & E. Grün 1998; E. Grün et al. 2000; M. Landgraf et al. 2000). Radar measurements obtained with the Arecibo Observatory (J. D. Mathews et al. 1999; D. D. Meisel et al. 2002a,b) constrained the flux of interstellar micrometeoroids (diameter  $< 10 - 100$   $\mu$ m) to be  $\sim 10^{-8}$  m<sup>-2</sup> s<sup>-1</sup>. The flux of 100  $\mu$ m interstellar meteoroids was constrained by the Canadian Meteor Orbit Radar (CMOR) (R. J. Weryk & P. Brown 2004) and  $> 20$   $\mu$ m sized interstellar meteoroids by the Advanced Meteor Orbit Radar (AMOR) (W. J. Baggaley et al. 1993; W. J. Baggaley 2000; A. D. Taylor et al. 1996). We refer the reader to V. J. Sterken et al. (2019) for a recent review.

The search for larger scale interstellar impactors has been debated for over a century; however, there remain no conclusive detections of interstellar meteors. In the early 1900s there was a claim that a substantial fraction of meteors in catalogues made by Von Niessl and Hoffmeister (G. Von Niessl & C. Hoffmeister 1925) were hyperbolic and therefore interstellar (W. J. Fisher 1928). However, this was refuted in the subsequent decades (M. Almond et al. 1951; E. J. Opik 1956; L. G. Jacchia & F. L. Whipple 1961; J. Štohl 1970; M. Hajduková 1993; M. Hajdukova 1994). Nondetections of interstellar meteoroids in optical data (R. L. Hawkes et al. 1999) from the Canadian Automated Meteor Observatory (CAMO) (R. Musci et al. 2012) and the IUA Meteor Date Center (J. Hajduková & T. Paulech 2002; M. Hajdukova 1994) have been used to constrain the overall flux. P. Wiegert et al. (2025) searched for interstellar events in the Global Meteor Network (GMN) and found no compelling candidates. While there are hyperbolic events in the Center for Near-Earth Object Studies databases (E. Peña-Asensio et al. 2022), there appears to be no compelling evidence that these fireballs were interstellar (J. Vaubaillon 2022; P. G. Brown & J. Borovička 2023; M. Hajduková et al. 2024). It has been demonstrated that measurement errors — and scattering via solar system planets in a small fraction of cases — accounts for hyperbolic events in most optical meteor networks (P. A. Wiegert 2014; M. Hajduková et al. 2014; M. Hajduková & L. Kornoš 2020; A. Egal et al. 2017; M. Hajduková et al. 2019; M. Hajduková & L. Kornoš 2020; M. Hajdukova et al. 2020) and of radar measured velocities of hyperbolic fireballs (W. J. Baggaley et al. 2007; R. Musci et al. 2012).

<sup>5</sup> While literature estimates of the nuclear radii of both objects vary, we report the average of all radii reported in Table 2 in D. Jewitt & D. Z. Seligman (2023).

Hyperbolic fireballs have been recorded in other databases. One hyperbolic event was observed by the Finnish Fireball Network with 1-sigma confidence (E. Peña-Asensio et al. 2024) and fifteen were observed by the European Fireball Network with 1-sigma confidence, including two with 3-sigma confidence (J. Borovička et al. 2022). Five candidate hyperbolic meteors have been identified with radar with 3-sigma confidence by CMOR (M. Froncisz et al. 2020). All these cases, however, are close to the parabolic limit, unlike 1I/‘Oumuamua and 2I/Borisov. Hyperbolic meteors are also reported in modern automated optical meteor network: hyperbolics make up i) 8% of all meteors recorded by the Global Meteor Network (GMN) (D. Vida et al. 2021) (updated on Jan 2025) and ii) 12% of all meteors in the Meteoroid Orbit Database v3.0 by Cameras for All-Sky Meteor Surveillance (CAMS) (P. Jenniskens et al. 2018). However, the researchers leading these networks have never claimed the detection of interstellar impactors.

The incoming extrasolar population remains poorly constrained across a broad size range, as linking interstellar dust and kilometer-scale objects to estimate the expected number of hyperbolic meteoroid impacts is not supported by meteor surveys (E. Peña-Asensio & D. Z. Seligman 2025). However, there have been efforts to calculate the distributions of interstellar objects passing through the Solar System. N. V. Cook et al. (2016) and T. Engelhardt et al. (2017b) produced some of the first synthetic populations of interstellar objects via direct numerical integrations. Other efforts to generate Monte Carlo simulations of interstellar objects include D. Seligman & G. Laughlin (2018); D. J. Hoover et al. (2022); S. A. Stern et al. (2024). D. Marčeta (2023) introduced the “probabilistic method” to generate synthetic interstellar objects. This method is orders of magnitude more computationally efficient than alternative approaches because it propagates trajectories analytically. It has been implemented to make predictions regarding the distribution of interstellar objects that should be detected with the forthcoming Rubin Observatory Legacy Survey of Space and Time (LSST) (D. Marčeta & D. Z. Seligman 2023; R. C. Dorsey et al. 2025) for a variety of assumptions regarding their kinematics (M. J. Hopkins et al. 2023; J. C. Forbes et al. 2024; M. J. Hopkins et al. 2025a).

In this paper we implement the probabilistic method to generate a population of Earth-impacting interstellar objects. The orders of magnitude increase in computational efficiency of the probabilistic method enables the generation a statistically robust synthetic population of Earth-impacting interstellar objects. Specifically,

we generate a population of  $> 10^{10}$  interstellar objects that give us a population of  $> 10^5$  Earth-impactors. We do not intend to make any claims about the presence or lack of interstellar meteors in extant data. Instead, these distributions are intended to be a useful and open-source tool to investigate Earth-impacting interstellar objects of macroscopic sizes, i.e., governed solely by gravity and unaffected by radiation.

## 2. SYNTHETIC POPULATION

In this section we describe the methodology to generate the synthetic population of interstellar objects and impactors. We implement the probabilistic method that was developed by D. Marčeta (2023) to generate all synthetic objects. The advent of the probabilistic method enables generation of a sufficient number of synthetic interstellar objects to obtain robust statistics on the subset of Earth-impactors.

### 2.1. Assumptions

In these calculations we purposefully do *not* assume a (i) size-frequency distribution, (ii) albedo distribution or, (iii) spatial number density of interstellar objects — all of which are entirely unconstrained. In other words, we do not attempt to predict the rate of interstellar impactors; we only calculate their expected and *unnormalized* distribution. It is worth noting that there are hints at what the size-frequency distribution of interstellar objects may be. For example A. Lecavelier des Etangs et al. (2022) inferred a similar size-frequency distribution of exocomets in the  $\beta$  Pictoris system as in Solar System populations of small bodies (B. Boe et al. 2019; G. Tanguy et al. 2006; C. Snodgrass et al. 2011; K. J. Meech et al. 2004; Y. R. Fernández et al. 2013; J. M. Bauer et al. 2017). However, it is unclear if the size-frequency-distribution of bound exocomets would be representative of the ejected subset. That being said, the distributions presented here are only applicable to interstellar objects that are large enough to not be affected by gas drag in the interstellar medium (B. T. Draine 2011; A. Moro-Martín & C. Norman 2022).

We assume that the interstellar objects have the same galactic kinematic as M-stars. This choice is admittedly somewhat arbitrary because the kinematics of interstellar objects is unconstrained. A detailed comparison of impactor properties for various galactic kinematics is outside of the scope of this work.

### 2.2. Orbit Generation

We calculate the subset of Earth-impacting interstellar objects as follows. First, test populations were generated within 1 au and propagated through time under

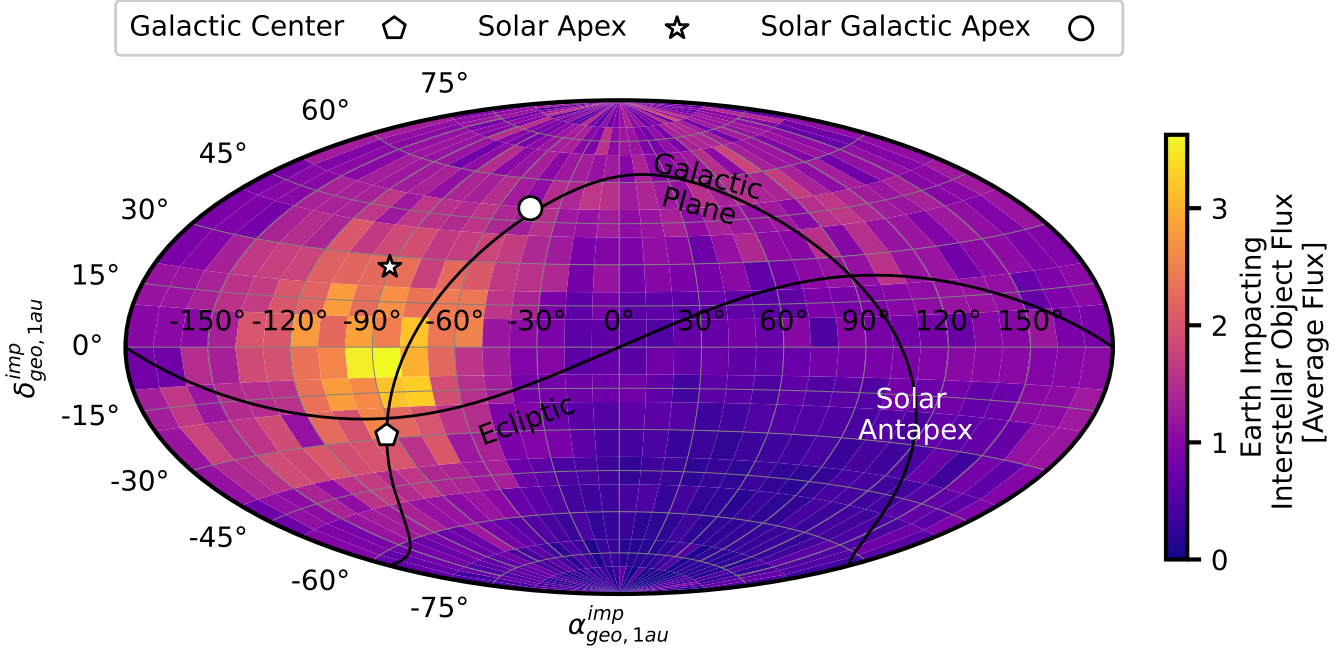


**Figure 1.** The radiants towards the Earth of impacting interstellar objects. Interstellar objects tend to impact the Earth in the directions of the solar apex and the galactic plane. Radiants are shown in the geocentric frame.

several assumed kinematic scenarios to determine the timescale for objects to leave this region. The residence time was found to be about 80 days in all cases. This duration represents the maximum time during which any ISO within 1 au could impact Earth. Next, the maximum heliocentric distance from which an ISO could reach 1 au within 80 days was calculated, assuming a speed of 100 km/s directed toward the Sun, yielding 4.5 au. Consequently, the full synthetic population was generated within 5.5 au. Finally, for each ISO orbit, the Minimum Orbit Intersection Distance (MOID) with Earth’s orbit was computed, and only those objects satisfying two conditions were retained: (1) their MOID was smaller than Earth’s effective radius, and (2) their orbital position allowed them to reach the intersection point within 80 days, corresponding to the approximate dynamical stationarity of the population near 1 au. In other words, interstellar objects in our synthetic population are considered impactors if they intersect the torus centered on the Sun with major/minor radius of  $1\text{au}/1R_{\oplus}^{\text{eff}}$  respectively, where  $R_{\oplus}^{\text{eff}}$  is the effective radius of the Earth, accounting for Earth’s gravitational focusing, and is defined as

$$R_{\oplus}^{\text{eff}} = R_{\oplus} \sqrt{1 + \left(\frac{v_{\text{geo}}^{\text{esc}}}{v_{\text{geo}}^{\text{imp}}}\right)^2}, \quad (1)$$

where  $R_{\oplus}$  is the physical radius of the Earth,  $v_{\text{geo}}^{\text{esc}}$  is Earth’s escape velocity, and  $v_{\text{geo}}^{\text{imp}}$  is the impact velocity.

The effective radius is calculated individually for each impact. For the remainder of this paper we refer to this volume as the “Earth-torus” for lack of a better nomenclature.

Therefore, our method generates  $\sim 1$  impactor for every  $\sim 8 \times 10^5$  synthetic objects. Robust statistics at the population level were achieved with a sample of Earth-impactors on the order of  $\sim 3.3 \times 10^4$ , enabling the identification of relevant structures in the population. This required the computation of  $\sim 2.6 \times 10^{10}$  synthetic interstellar objects, which demonstrates the prerequisite for the computational efficiency of the probabilistic method.

The probabilistic method incorporates gravitational focusing from the Sun, but *not* from the Earth. Technically, the mutual gravity from both the Earth and the Sun should be incorporated via direct numerical integration to evaluate this population. However, this is not feasible computationally for the total number of synthetic objects required to generate a substantive impactor population. However, meteor databases typically provide both the geocentric and apparent/observed radiants and velocity, as well as osculating orbital elements. Therefore, the distributions presented in this paper will still be straightforward to compare with meteor databases.

### 2.3. Terminology

We briefly describe some terminology here that we will implement throughout the remainder of this pa-

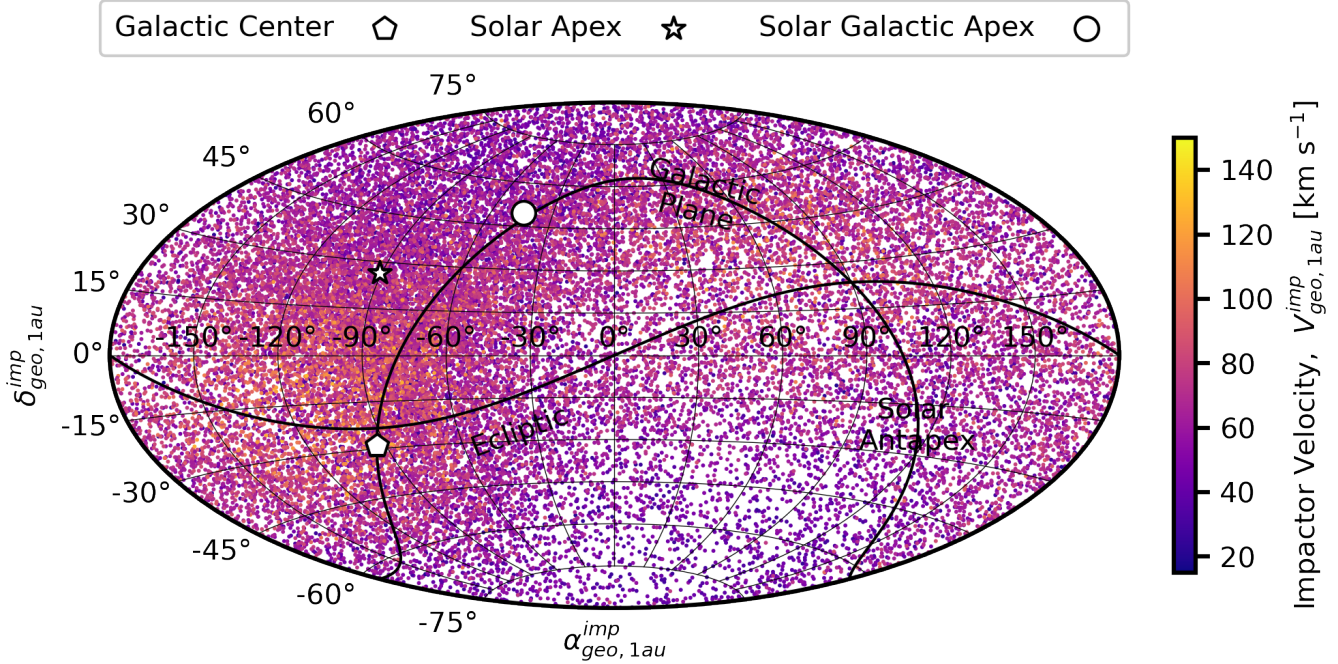


**Figure 2.** Interstellar objects impact the Earth with higher velocity when approaching from the solar apex and the galactic plane. Impactor velocity is calculated in the geocentric frame.

per to avoid confusion. We differentiate between the geocentric and heliocentric frame for a given parameter  $X$  with subscripts  $X_{geo}$  and  $X_{hel}$ . In this paper, heliocentric means ecliptic Sun-centered while geocentric means equatorial Earth-centered. We distinguish between a parameter that has been affected (at 1 au) and has not been affected by gravitational focusing of the Sun with subscripts  $X_{1au}$  and  $X_{\infty}$  respectively. Finally, we differentiate between the interstellar impactors and the overall interstellar population with the superscript  $X^{imp}$  and  $X^{all}$ . For example, the velocity of the impactor population in the geocentric frame at infinity would be  $V_{geo,\infty}^{imp}$ .

All of the eccentricities described throughout the paper are hyperbolic by construction. We routinely describe eccentricities that are close to 1 ( $e \sim 1 - 2$ ) as low-eccentricity, not to be confused with near-circular ( $e \sim 0$ ).

Finally, in this paper we describe velocity vectors and magnitudes often and interchangeably. For the remainder of this paper, a quantity is only assumed to be a vector if it has the vector arrow denotation. For example  $\vec{V}$  is the velocity vector, but  $V$  denotes only the magnitude of the vector.

### 3. DISTRIBUTION OF INTERSTELLAR IMPACTORS

In this section we present the distribution of Earth-impacting interstellar objects. In the following three

subsections we describe the orbits, seasonal variability, and Earth-locations of the population.

#### 3.1. Orbits of Impactors

In Figure 1 we show the relative flux of Earth-impacting interstellar objects as a function of their radiants in geocentric equatorial J2000. There are flux enhancements/deficits of a factor of  $\sim 2$  compared to the mean in the direction of the solar apex/antapex. There is also an enhancement of impactors in the direction of the galactic plane. The faster objects tend to cluster in the direction of the solar apex and the galactic plane (Figure 2). It should be noted that this clustering is not exclusive to interstellar impactors and is seen with all impactors.

The cells shown in Figure 1 are evenly spaced in right ascension ( $\alpha$ ) and declination ( $\delta$ ), and therefore have *uneven* surface area. We correct for this geometric effect by dividing the number of objects in each cell by its normalized surface area,  $\sigma_{ij}$ , given by:

$$\sigma_{ij} = |\alpha_{i+1/2} - \alpha_{i-1/2}| |\sin \delta_{j+1/2} - \sin \delta_{j-1/2}| \quad (2)$$

In Equation 2, the subscripts  $i$  and  $j$  correspond to the horizontal and vertical indices of the grid respectively. Figures 1 and 2 use an Aitoff projection.

In Figure 3 we show the distributions of velocities of the Earth-impactors and of the entire interstellar population. The impactors peak at geocentric velocities of

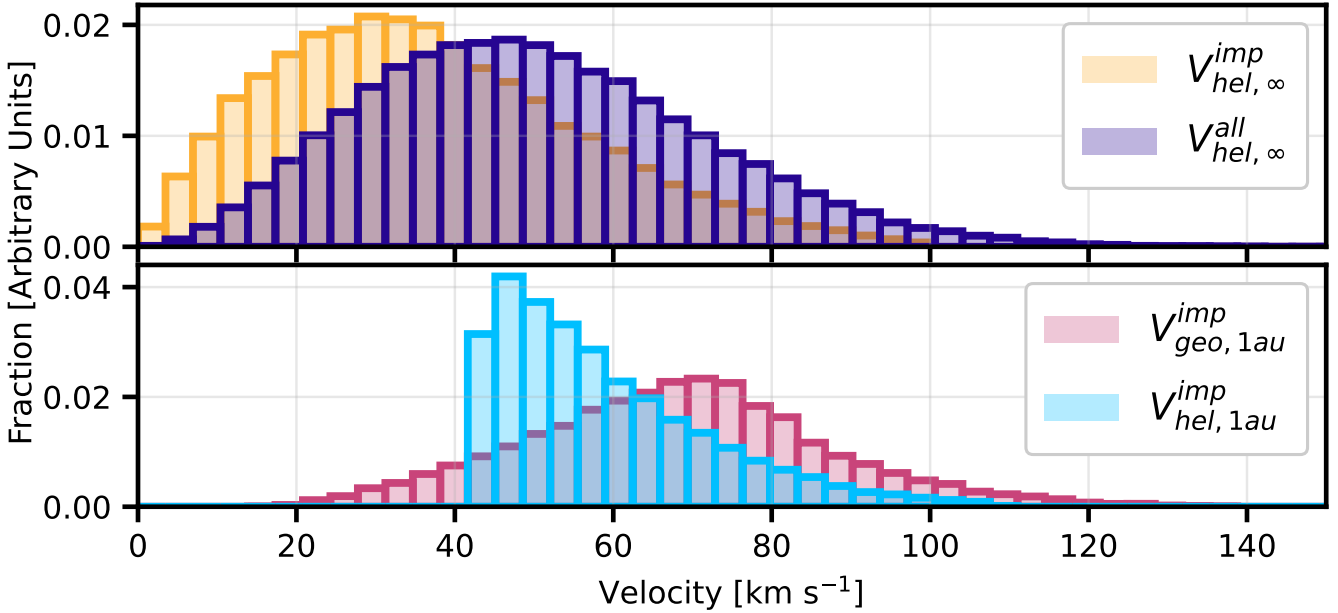


**Figure 3.** The distribution of velocities of Earth-impacting interstellar objects are distinct from the overall interstellar object population. The addition of the Earth's velocity shifts the lognormal distribution to higher median values for the geocentric frame.

$\sim 72 \text{ km s}^{-1}$ . This corresponds to the maximum collisional velocity of two solar system objects which interstellar particles may exceed (M. Hajdukova et al. 2020). The interstellar population should encounter the Solar System with the mean velocity of the Sun with respect to the local standard of rest. Therefore, the heliocentric velocity distribution at 1 au should peak at  $\sim 45 \text{ km s}^{-1}$  after considering the solar acceleration. The slowest impactors should encounter the Earth from behind with geocentric velocities of  $12 \text{ km s}^{-1}$  ( $42 - 30 \text{ km s}^{-1}$ )<sup>6</sup>.

It is somewhat surprising that the geocentric impactor distribution peaks at  $\sim 72 \text{ km s}^{-1}$ . Intuitively, we would expect that the geocentric velocities of  $\sim 75$  ( $45 + 30 \text{ km s}^{-1}$ ) and  $\sim 15 \text{ km s}^{-1}$  ( $45 - 30 \text{ km s}^{-1}$ ) would have roughly the same probability. However, it is much more likely for an interstellar impact to have higher velocities. The relative collision velocity,  $\vec{V}_{rel,1au}$  (which is effectively our  $V_{geo,1au}^{imp}$ ), is given by:

$$|\vec{V}_{rel,1au}| = \sqrt{|\vec{V}_{hel,1au}|^2 - 2|\vec{V}_{hel,1au}||\vec{V}_\oplus| \cos \psi + |\vec{V}_\oplus|^2}. \quad (3)$$

In Equation 3,  $\vec{V}_{hel,1au}$  and  $\vec{V}_\oplus$  are the heliocentric velocity vectors of the interstellar object and the Earth respectively, while  $\psi$  is the angle between them. It is evident from Equation 3 that a collision with low rela-

tive velocity only occurs when the Earth and the interstellar object move in the same direction, or for small  $\psi$ . In other words, low relative velocities only occur when the interstellar object moves in the ecliptic plane and directly impacts the Earth from behind. As the relative velocity increases, the number of possible combinations that can result in a given relative velocity increases. Therefore the distribution of velocities is naturally skewed towards higher values.

The median *heliocentric* velocity of the impactors is slower than that of the overall interstellar population. We reiterate for clarity that in this paper heliocentric means ecliptic Sun-centered while geocentric means equatorial Earth-centered. This excess of slowly moving impactors can be readily explained. These objects have low-eccentricity orbits; it is evident in Figure 4 that the vast majority of objects have eccentricity close to  $e = 1$ . These low-eccentricity orbits have corresponding slow velocities at infinity,  $V_{hel,\infty} \simeq 0 \text{ km s}^{-1}$  (Figure 6). These objects spend more time in a given heliocentric range than faster objects and therefore experience stronger gravitational focusing. For example, an object with  $q = 1 \text{ au}$  and  $V_{hel,\infty} = 0 \text{ km s}^{-1}$  spends  $\sim 30\%$  more time in the vicinity of the Earth compared to an object with  $q = 1 \text{ au}$  and  $V_{hel,\infty} = 25 \text{ km s}^{-1}$ . Therefore, low-eccentricity objects are more likely to enter the Earth-torus.

In conclusion, the slow impactors have essentially the same velocity at 1 au ( $\sim 42-43 \text{ km s}^{-1}$ ) even if they have

<sup>6</sup> The escape velocity of the Solar System at 1 au minus the heliocentric velocity of the Earth.

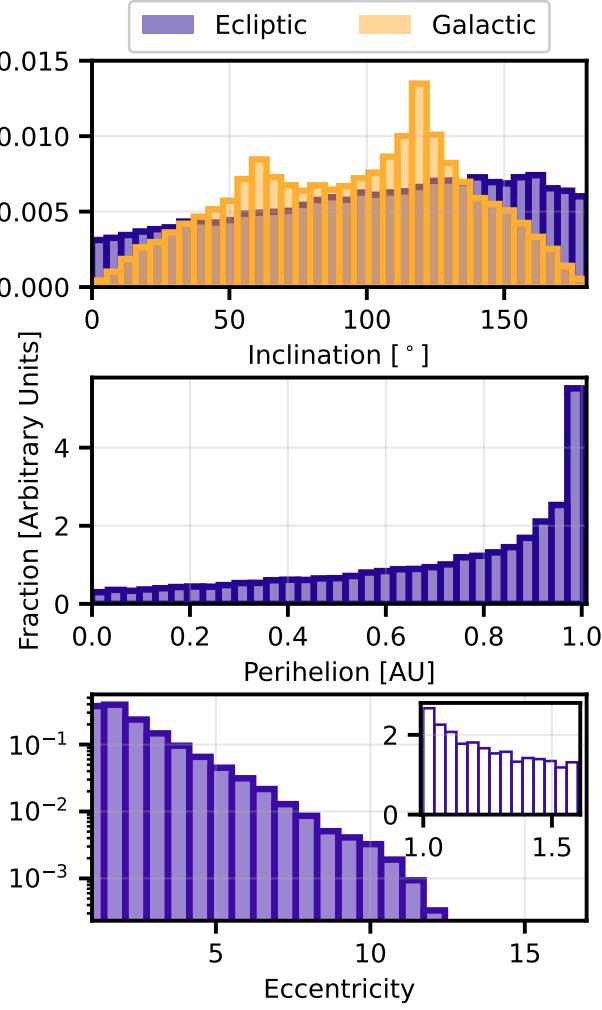


**Figure 4.** Earth-impacting interstellar objects are significantly more likely to have perihelia close to the Earth and hyperbolic orbits near the low-eccentricity limit. The inclination distribution measured with respect to the ecliptic is uniform in angular space. In physical space, there is a larger fraction of impactor orbits in the ecliptic plane. This is because prograde and retrograde ecliptic interstellar objects are significantly more likely to cross the Earth-torus. The inset in the lower panel shows the low-eccentricity limit and has the same axes.

differences of up to  $9 \text{ km s}^{-1}$  at infinity. This implies that the majority of interstellar objects that impact the Earth should do so just slightly above the escape velocity from the Solar System at 1 au. It is worth noting that our choice of adopting M-star kinematics diminishes this effect; if we had used the O/B or G kinematics, the distribution would be even more concentrated towards the low-eccentricity limit because they are slower.

In Figures 4 and 5 we show the orbital elements of the Earth-impactors. The majority of Earth-impactors have low-eccentricity orbits with perihelia close to the Earth-

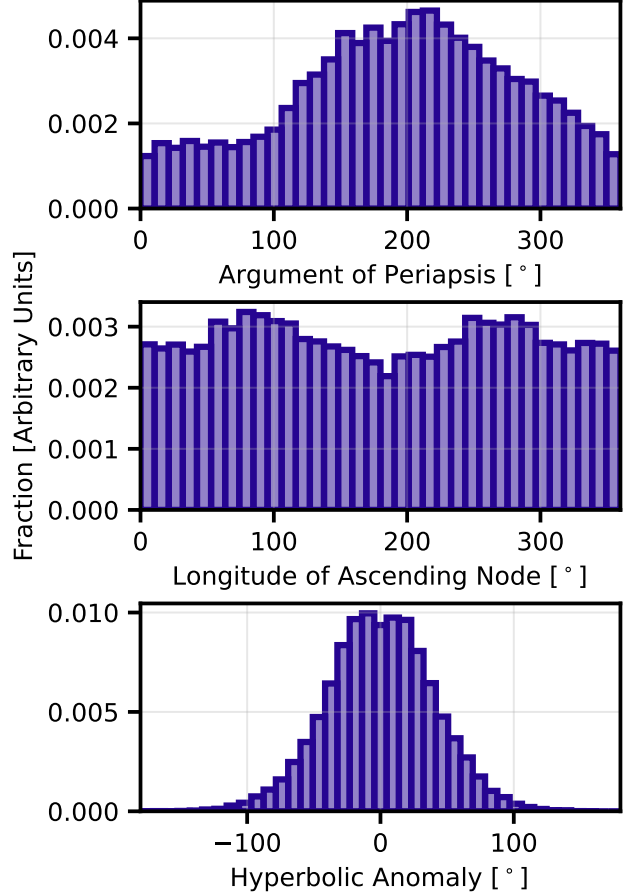


**Figure 5.** The distributions of longitude of ascending node, argument of periapsis, and hyperbolic anomaly of the impactors are approximately symmetric. These distributions are similar to those in the overall interstellar populations (D. Marčeta 2023).

distance from the Sun. The prevalence of  $q \sim 1 \text{ au}$  perihelion distances was explained in D. Marčeta (2023). The  $q \sim 1 \text{ au}$  impactors in our population correspond to the outer limiting trajectory in Figure 1 of that paper, where the radial velocity in the shell is zero. The relative number density is obtained in Equation 12 of that paper by dividing the flux by the area of the shell and the radial velocity. This results in a predominance of orbits with perihelion close to the outer radius of a given shell for every shell. These outer most orbits are therefore the slowest moving objects in the radial direction (for a given shell), meaning they spend the most time inside the shell compared to orbits with lower perihelia. Therefore, they are the most likely orbits to impact.

The inclination distribution of impactors differs significantly from that of the overall population. As shown in Figure 7, it is closely linked to the perihelion distance. This bivariate histogram shows only the distribution of

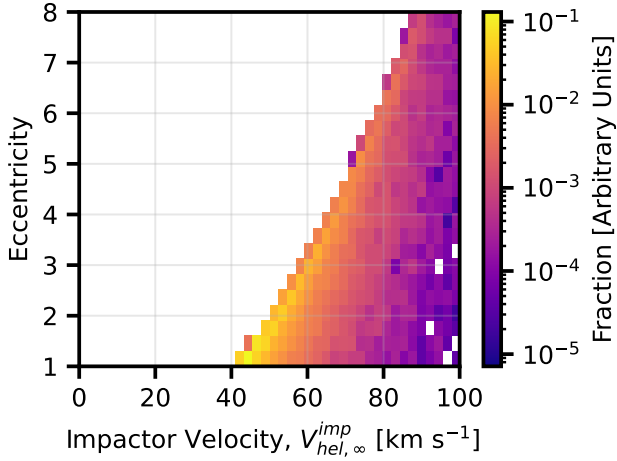


**Figure 6.** The distribution of velocity of impactors correlates with eccentricity. The low-eccentricity objects all have low velocities at infinity. Note that the zoomed-in axes do not show the entire range of eccentricities and velocities in the impactor population.

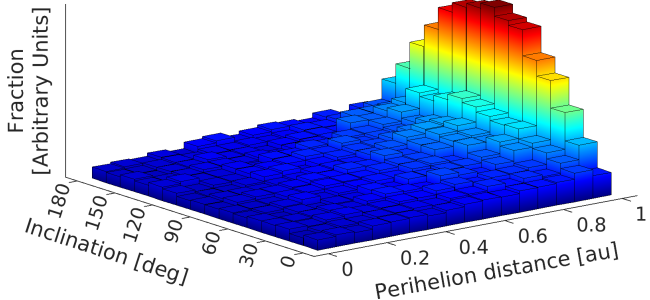


**Figure 7.** Unweighted inclination distribution of earth-impacting interstellar objects becomes sinusoidal/uniform at larger/smaller perihelion distances.

all objects that entered the Earth-torus during the analyzed period, without accounting for their impact probability, which is discussed later in this section. With increasing perihelion distance, the inclination distribution approaches a sinusoidal form, consistent with the overall population. Conversely, for smaller perihelion distances, the distribution becomes increasingly uniform.

This behavior arises from a geometrical selection effect illustrated in Figure 8. For small values of  $q$ , the orbit intersects Earth's orbital path almost perpendicular. In this regime, the range of argument of perihelion values that allow an intersection depends strongly on inclination. At low inclinations, the intersection arc along Earth's orbit is longer, permitting a wider range of argument-of-perihelion values that produce a crossing. For larger  $q$ , the orbit intersects Earth's orbital path more tangentially, and the impact condition becomes less sensitive to inclination, since similar range

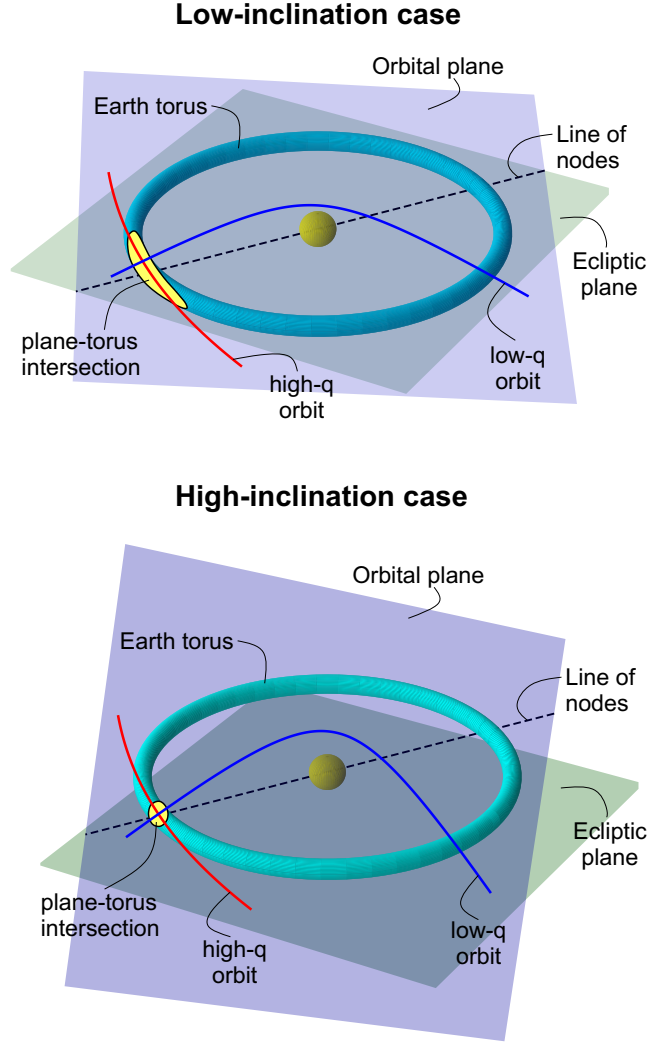


**Figure 8.** Geometrical selection effect illustrated for low inclination (upper panel) and high inclination (lower panel). Low- $q$  orbits intersect Earth's path nearly perpendicular, while high- $q$  orbits intersect nearly tangentially. The length of the intersection arc depends only on inclination, having a strong effect for low- $q$  orbits but a negligible effect for high- $q$  orbits.

of argument of perihelion values still satisfies the intersection criterion. As a result, low-inclination orbits are favored, and the resulting inclination distribution becomes flatter than the original one.

An additional reason why orbits close to the ecliptic are favored is that objects on such orbits have a longer residence time within the Earth-torus. This increases their likelihood of impact, as they can encounter Earth over a larger fraction of its orbit. Furthermore, since the impact flux is proportional to  $v_{geo,1,au}^{imp}$ , all distributions are skewed toward retrograde objects, as is clearly visible in the top panel of Figure 4. To account for this

effect, we propagated the orbits of all impactors and calculated their residence time ( $t_{\text{res}}$ ) inside the Earth-torus. Then, all the distributions shown in Figures 4 and 5 were weighted by  $t_{\text{res}} \cdot v_{\text{geo},1\text{au}}^{\text{imp}}$ .

The inclination distribution of impactors with respect to the galactic plane has two peaks at  $i \sim 60^\circ$  and  $i \sim 120^\circ$  (Figure 4). These two peaks correspond to direct and retrograde interstellar objects in the ecliptic plane whose obliquity to the galactic plane is  $60^\circ$ . The right peak is more pronounced because it corresponds to retrograde objects. This occurs because the impact flux is proportional to  $v_{\text{geo}}$ , as mentioned. This effect also causes the inclination distribution with respect to the ecliptic plane to be asymmetric toward retrograde objects.

The remaining three orbital element angles (Figure 5) are roughly symmetric. The distributions of argument of periapsis and longitude of the ascending node are bimodal. All three distributions are similar to those for the overall interstellar population, as can be seen upon visual comparison with Figure 9 in D. Marčeta (2023).

### 3.2. Seasonal Dependence

In this subsection we present the seasonal dependence of the interstellar impactor distributions. In Figure 9 we show the radiants of Earth-impacting interstellar objects as a function of solar longitude and velocity. The calendar month is calculated assuming that the Earth has the same ecliptic longitude as the interstellar object when it crosses the Earth-torus. The seasons are defined based on the Northern hemisphere. To convert the solar longitude to month, we neglect the fact that the solar longitude is slowly drifting with respect to the seasons. For simplicity, we plot October, January, April, and July as  $\pm\pi, -\pi/2, 0$ , and  $\pi/2$ .

There is significant substructure in the parameter space spanning radiants, impactor velocity, and solar longitude implying significant seasonal dependence of impactors. For example, the fastest interstellar objects impact in the spring when the Earth is moving towards the apex.

However, interstellar objects are overall more likely to impact when the Earth is in the direction of the antapex which occurs in winter. In Figure 10 we show the distribution of total relative impacts as a function of solar longitude. The flux increases during winter, when the Earth is near the solar antapex, as the Sun acts as a gravitational lens that focuses a larger number of particle trajectories toward Earth's orbit, in agreement with P. Strub et al. (2019).

We provide a discussion of the physical explanation for this bias. Consider two trajectories of interstellar

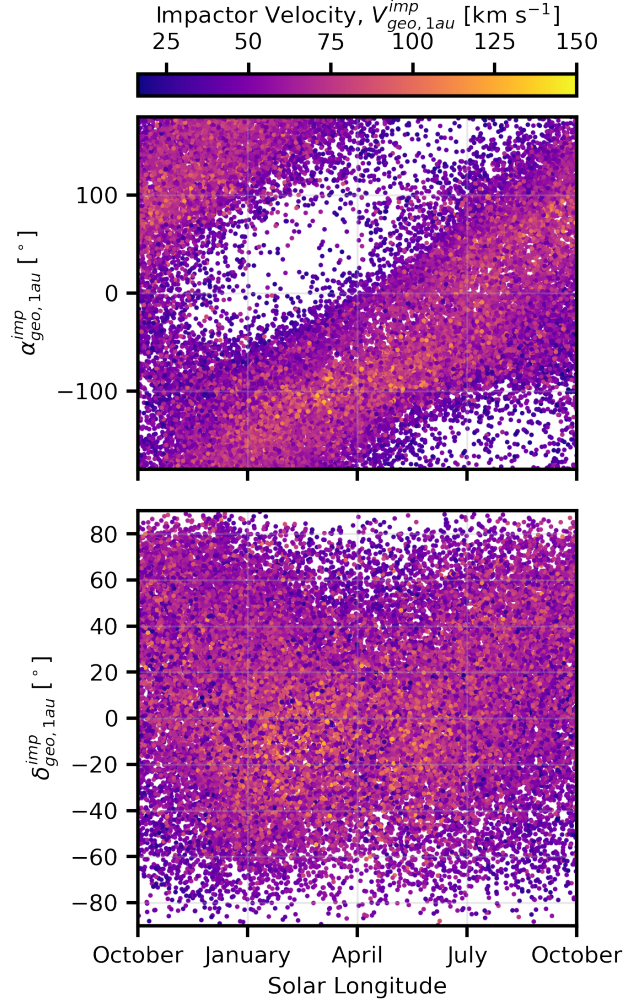


**Figure 9.** Faster interstellar objects are more likely to impact the Earth in the spring when the Earth is moving towards the apex. The declination distribution of high velocity impactors mirrors the ecliptic plane. Velocities shown are calculated in the geocentric frame

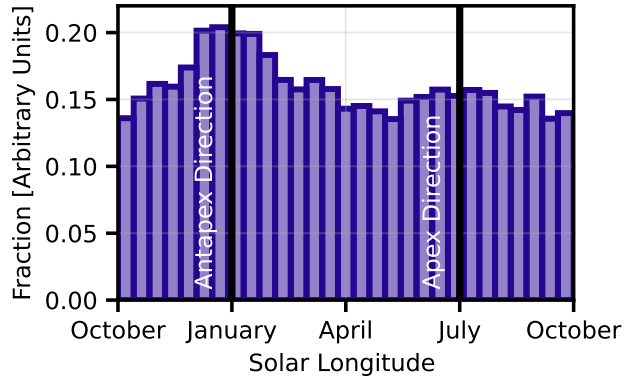


**Figure 10.** Interstellar objects are more likely to impact the Earth in the winter than the spring.

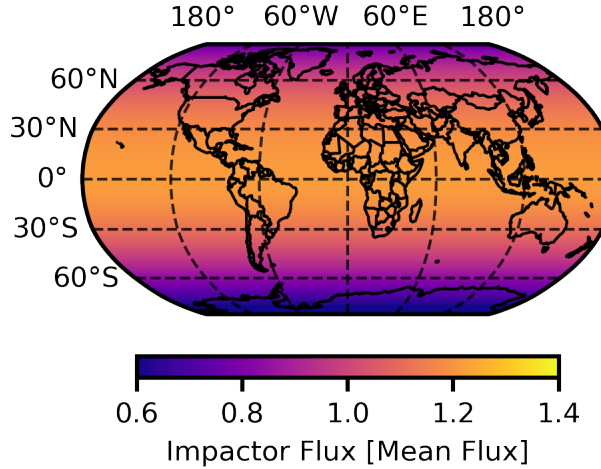


**Figure 11.** Interstellar objects are more likely to impact the Earth at low latitudes close to the equator. There is a slight preference for impactors in the Northern hemisphere.

objects arriving in the direction of the apex on the near and far side of the Sun compared to the motion of the Earth. An interstellar object coming from the far side of the Sun in the apex direction has a higher chance of impact because it collides after perihelion. This means it can originate from a slightly larger impact parameter; moreover, the number of interstellar objects is linearly proportional to the impact parameter (D. Marčeta 2023; D. Z. Seligman & A. Moro-Martín 2023). In this case, the impact can occur at a larger impact parameter and perihelion distance compared to the near side case, which will collide before perihelion.

There is also a possibility that an apex-side impact occurs after perihelion. In this scenario there are two post-perihelion impacts but once again the antapex impact is more likely to occur due to significantly larger impact parameter and perihelion distance. In other words, impacts when the Earth is close to the antapex have experienced the Solar gravitational focusing for longer; a similar case for bound objects was described in A. V. Moorhead et al. (2020). They can therefore arrive from a greater region in space, increasing the number of them that can bend their trajectory and impact the Earth. In our simulations the mean perihelion distance for apex-side impacts is 0.51 au while for antapex-side impacts the mean perihelion is  $q = 0.77$  au. Additionally, the largest perihelion distance for apex-side impacts is 0.69 au while for antapex side impacts it is 1 au (which is the largest possible perihelion distance for an impact to occur anywhere).

### 3.3. Latitudinal Distribution of Impacts

In Figure 11 we show the relative flux of interstellar impactors on the surface of the Earth. To calculate this distribution we take into account the fact that a given radiant can impact at multiple locations on the Earth. Specifically, a single radiant corresponds to an entire hemisphere of possible approach directions comprised of orbits parallel to that radiant. To calculate this distribution we compute every latitude and longitude that correspond to the hemisphere defined by a given radiant, and then sum over all radiants. The inclination of the Earth’s pole with respect to the ecliptic is accounted for when transforming between ecliptic and equatorial reference frames. The gravitational influence of the Earth is not incorporated into this calculation. Figure 11 is therefore only intended to depict a *tentative* latitudinal dependence as opposed to an exact positional prediction. Interstellar objects are more likely to hit the Earth at low latitudes close to the equator with a slight preference for the Northern hemisphere. Figure 11 uses a Robinson projection.

## 4. DISCUSSION

In this paper we generated a synthetic population of Earth-impacting interstellar objects with the recently developed probabilistic method (D. Marčeta 2023). The orders of magnitude increase in computational efficiency of this methodology enabled the generation of a statistically robust population of Earth-impactors. In order to generate  $\sim 3.3 \times 10^4$  Earth-impactors, we computed  $\sim 2.6 \times 10^{10}$  synthetic overall objects.

These simulations revealed several salient properties of the Earth-impacting interstellar objects which can be summarized as follows:

1. Earth-impacting interstellar objects are most likely to approach from the solar apex and the galactic plane.
2. The fastest Earth-impacting interstellar objects approach from the galactic plane and solar apex.
3. Earth-impacting interstellar objects are typically slower than the overall interstellar population.
4. Earth-impacting interstellar objects typically have hyperbolic, low-eccentricity orbits.
5. Earth-impacting interstellar objects are likely to have orbits within the ecliptic plane, predominantly with retrograde motion. Earth-impacting interstellar objects exhibit a sinusoidal inclination distribution for high  $q$ , similar to the overall population, but tend toward a uniform distribution for low  $q$ .

6. The fastest interstellar impactors collide in the spring when the Earth is moving towards the solar apex.
7. Interstellar objects are more likely to impact the Earth in the winter when the Earth is in the direction of the antapex.
8. Interstellar objects are more likely to impact the Earth close to the equator and in the Northern hemisphere.

Here we highlight caveats and areas of future works. These distributions are only applicable for interstellar objects that have M-stars kinematics. Different assumed kinematics should change the distributions presented in this paper. The salient features summarized in this section presumably also apply to different kinematics, perhaps to a muted or more distinct overall effect. It would be useful to perform similar analyses for different kinematics, although this is outside of the scope of this paper. For example, [C. R. Gregg & P. A. Wiegert \(2025\)](#) argued that interstellar meteors from  $\alpha$ -Centauri should be distinct in their average position and higher velocities  $\sim 53 \text{ km s}^{-1}$  at 1 au. Finally, these distributions are only applicable to objects sufficiently large to not be affected by gas drag in the interstellar medium.

In this paper we intentionally do not make any definitive predictions about the rates of interstellar impactors. In turn, we also do not make any claims regarding the presence or lack of interstellar meteors in extent data. The distribution of Earth-impactors are open source, and intended to be a useful tool for other researchers

to investigate Earth-impacting interstellar objects of macroscopic sizes.

## 5. ACKNOWLEDGMENTS

We thank the anonymous reviewer for insightful comments and constructive suggestions that strengthened the scientific content of this manuscript. We thank Mariá Hajduková for providing an informal review of the manuscript upon submission.

We thank Héctor Socas-Navarro, Brian O’Shea, Lia Coralles, Adina Feinstein, Garrett Levine, Amanda Gill, and Jason Kohn for useful conversations.

D.Z.S. is supported by an NSF Astronomy and Astrophysics Postdoctoral Fellowship under award AST-2303553. This research award is partially funded by a generous gift of Charles Simonyi to the NSF Division of Astronomical Sciences. The award is made in recognition of significant contributions to Rubin Observatory’s Legacy Survey of Space and Time.

D.M. acknowledges support by the Science Fund of the Republic of Serbia, GRANT No 7453, Demystifying enigmatic visitors of the near-Earth region (ENIGMA).

E.P.-A. acknowledges financial support from the LUMIO project, funded by the Agenzia Spaziale Italiana (2024-6-HH.0).

## 6. CONTRIBUTION

All authors contributed equally to this manuscript. D.Z.S. led the paper writing and figure generation, and contributed to interpretation of data. D. M. performed the numerical simulations, led the interpretation of data, and contributed to figure generation. E. P. A. contributed to manuscript writing, interpretation of data, and figure generation.

## REFERENCES

Alarcon, M. R., Serra-Ricart, M., Licandro, J., et al. 2025, Deep g'-band Imaging of Interstellar Comet 3I/ATLAS from the Two-meter Twin Telescope (TTT), *The Astronomer’s Telegram*, 17264, 1

Almeida-Fernandes, F., & Rocha-Pinto, H. J. 2018, A kinematical age for the interstellar object 1I/‘Oumuamua, *MNRAS*, 480, 4903, doi: [10.1093/mnras/sty2202](https://doi.org/10.1093/mnras/sty2202)

Almond, M., Davies, J. G., & Lovell, A. C. B. 1951, The velocity distribution of sporadic meteors. I., *MNRAS*, 111, 585, doi: [10.1093/mnras/111.6.585](https://doi.org/10.1093/mnras/111.6.585)

Aravind, K., Ganesh, S., Venkataramani, K., et al. 2021, Activity of the first interstellar comet 2I/Borisov around perihelion: results from Indian observatories, *MNRAS*, 502, 3491, doi: [10.1093/mnras/stab084](https://doi.org/10.1093/mnras/stab084)

Baggaley, W. J. 2000, Advanced Meteor Orbit Radar observations of interstellar meteoroids, *J. Geophys. Res.*, 105, 10353, doi: [10.1029/1999JA900383](https://doi.org/10.1029/1999JA900383)

Baggaley, W. J., Marsh, S. H., & Close, S. 2007, in *ESA Special Publication*, Vol. 643, *Dust in Planetary Systems*, ed. H. Krueger & A. Graps, 27–32

Baggaley, W. J., Taylor, A. D., & Steel, D. I. 1993, in *Meteoroids and their Parent Bodies*, ed. J. Stohl & I. P. Williams, 53

Bannister, M. T., Schwamb, M. E., Fraser, W. C., et al. 2017, Col-OSSOS: Colors of the Interstellar Planetesimal 1I/‘Oumuamua, *ApJL*, 851, L38, doi: [10.3847/2041-8213/aaa07c](https://doi.org/10.3847/2041-8213/aaa07c)

Bannister, M. T., Opitom, C., Fitzsimmons, A., et al. 2020, Interstellar comet 2I/Borisov as seen by MUSE: C<sub>2</sub>, NH<sub>2</sub> and red CN detections, *arXiv e-prints*, arXiv:2001.11605. <https://arxiv.org/abs/2001.11605>

Bauer, J. M., Grav, T., Fernández, Y. R., et al. 2017, Debiasing the NEOWISE Cryogenic Mission Comet Populations, *AJ*, 154, 53, doi: [10.3847/1538-3881/aa72df](https://doi.org/10.3847/1538-3881/aa72df)

Belton, M. J. S., Hainaut, O. R., Meech, K. J., et al. 2018, The Excited Spin State of 1I/2017 U1 Oumuamua, *ApJL*, 856, L21, doi: [10.3847/2041-8213/aab370](https://doi.org/10.3847/2041-8213/aab370)

Bodewits, D., Noonan, J. W., Feldman, P. D., et al. 2020, The carbon monoxide-rich interstellar comet 2I/Borisov, *Nature Astronomy*, 4, 867, doi: [10.1038/s41550-020-1095-2](https://doi.org/10.1038/s41550-020-1095-2)

Boe, B., Jedicke, R., Meech, K. J., et al. 2019, The orbit and size-frequency distribution of long period comets observed by Pan-STARRS1, *Icarus*, 333, 252, doi: [10.1016/j.icarus.2019.05.034](https://doi.org/10.1016/j.icarus.2019.05.034)

Borisov, G., Durig, D. T., Sato, H., et al. 2019, Comet C/2019 Q4 (Borisov), *Central Bureau Electronic Telegrams*, 4666, 1

Borovička, J., Spurný, P., & Shrbený, L. 2022, Data on 824 fireballs observed by the digital cameras of the European Fireball Network in 2017-2018. II. Analysis of orbital and physical properties of centimeter-sized meteoroids, *A&A*, 667, A158, doi: [10.1051/0004-6361/202244197](https://doi.org/10.1051/0004-6361/202244197)

Brown, P. G., & Borovička, J. 2023, On the Proposed Interstellar Origin of the USG 20140108 Fireball, *ApJ*, 953, 167, doi: [10.3847/1538-4357/ace421](https://doi.org/10.3847/1538-4357/ace421)

Cabot, S. H. C., & Laughlin, G. 2022, Identifying Interstellar Object Impact Craters, *PSJ*, 3, 172, doi: [10.3847/PSJ/ac77e9](https://doi.org/10.3847/PSJ/ac77e9)

Chandler, C. O., Bernardinelli, P. H., Jurić, M., et al. 2025, NSF-DOE Vera C. Rubin Observatory Observations of Interstellar Comet 3I/ATLAS (C/2025 N1), *arXiv e-prints*, arXiv:2507.13409. <https://arxiv.org/abs/2507.13409>

Chang, D., Hsieh, C.-H., & Laughlin, G. 2023, Constraints to Efficiently Find Interstellar Object Generated Craters on the Moon, *Research Notes of the American Astronomical Society*, 7, 228, doi: [10.3847/2515-5172/ad0731](https://doi.org/10.3847/2515-5172/ad0731)

Cook, N. V., Ragozzine, D., Granvik, M., & Stephens, D. C. 2016, Realistic Detectability of Close Interstellar Comets, *ApJ*, 825, 51, doi: [10.3847/0004-637X/825/1/51](https://doi.org/10.3847/0004-637X/825/1/51)

Cordiner, M. A., Milam, S. N., Biver, N., et al. 2020, Unusually high CO abundance of the first active interstellar comet, *Nature Astronomy*, 4, 861, doi: [10.1038/s41550-020-1087-2](https://doi.org/10.1038/s41550-020-1087-2)

Cremonese, G., Fulle, M., Cambianica, P., et al. 2020, Dust Environment Model of the Interstellar Comet 2I/Borisov, *ApJL*, 893, L12, doi: [10.3847/2041-8213/ab8455](https://doi.org/10.3847/2041-8213/ab8455)

de la Fuente Marcos, R., Licandro, J., Alarcon, M. R., et al. 2025, Assessing interstellar comet 3I/ATLAS with the 10.4 m Gran Telescopio Canarias and the Two-meter Twin Telescope, *arXiv e-prints*, arXiv:2507.12922. <https://arxiv.org/abs/2507.12922>

Denneau, L., Siverd, R., Tonry, J., et al. 2025, 3I/ATLAS = C/2025 N1 (ATLAS), *MPEC*

Do, A., Tucker, M. A., & Tonry, J. 2018, Interstellar Interlopers: Number Density and Origin of ‘Oumuamua-like Objects, *ApJL*, 855, L10, doi: [10.3847/2041-8213/aaae67](https://doi.org/10.3847/2041-8213/aaae67)

Dorsey, R. C., Hopkins, M. J., Bannister, M. T., et al. 2025, The visibility of the Ōtautahi-Oxford interstellar object population model in LSST, *arXiv e-prints*, arXiv:2502.16741, doi: [10.48550/arXiv.2502.16741](https://doi.org/10.48550/arXiv.2502.16741)

Drahus, M., Yang, B., Lis, D. C., & Jewitt, D. 2017, New Limits to CO Outgassing in Centaurs, *MNRAS*, 468, 2897, doi: [10.1093/mnras/stw2227](https://doi.org/10.1093/mnras/stw2227)

Draine, B. T. 2011, Physics of the Interstellar and Intergalactic Medium ()

Egal, A., Gural, P. S., Vaubaillon, J., Colas, F., & Thuillot, W. 2017, The challenge associated with the robust computation of meteor velocities from video and photographic records, *Icarus*, 294, 43, doi: [10.1016/j.icarus.2017.04.024](https://doi.org/10.1016/j.icarus.2017.04.024)

Engelhardt, T., Jedicke, R., Vereš, P., et al. 2017a, An Observational Upper Limit on the Interstellar Number Density of Asteroids and Comets, *AJ*, 153, 133, doi: [10.3847/1538-3881/aa5c8a](https://doi.org/10.3847/1538-3881/aa5c8a)

Engelhardt, T., Jedicke, R., Vereš, P., et al. 2017b, An Observational Upper Limit on the Interstellar Number Density of Asteroids and Comets, *AJ*, 153, 133, doi: [10.3847/1538-3881/aa5c8a](https://doi.org/10.3847/1538-3881/aa5c8a)

Farnocchia, D., Seligman, D. Z., Granvik, M., et al. 2023, (523599) 2003 RM: The Asteroid that Wanted to be a Comet, *PSJ*, 4, 29, doi: [10.3847/PSJ/acb25b](https://doi.org/10.3847/PSJ/acb25b)

Feng, F., & Jones, H. R. A. 2018, ‘Oumuamua as a Messenger from the Local Association, *ApJL*, 852, L27, doi: [10.3847/2041-8213/aaa404](https://doi.org/10.3847/2041-8213/aaa404)

Fernández, Y. R., Kelley, M. S., Lamy, P. L., et al. 2013, Thermal properties, sizes, and size distribution of Jupiter-family cometary nuclei, *Icarus*, 226, 1138, doi: [10.1016/j.icarus.2013.07.021](https://doi.org/10.1016/j.icarus.2013.07.021)

Fisher, W. J. 1928, Remarks on the Fireball Catalogue of von Niessl and Hoffmeister., Harvard College Observatory Circular, 331, 1

Fitzsimmons, A., Meech, K., Matrà, L., & Pfalzner, S. 2023, Interstellar Objects and Exocomets, arXiv e-prints, arXiv:2303.17980, doi: [10.48550/arXiv.2303.17980](https://doi.org/10.48550/arXiv.2303.17980)

Fitzsimmons, A., Snodgrass, C., Rozitis, B., et al. 2018, Spectroscopy and thermal modelling of the first interstellar object 1I/2017 U1 ‘Oumuamua, *Nature Astronomy*, 2, 133, doi: [10.1038/s41550-017-0361-4](https://doi.org/10.1038/s41550-017-0361-4)

Fitzsimmons, A., Hainaut, O., Meech, K. J., et al. 2019, Detection of CN Gas in Interstellar Object 2I/Borisov, *ApJL*, 885, L9, doi: [10.3847/2041-8213/ab49fc](https://doi.org/10.3847/2041-8213/ab49fc)

Forbes, J. C., Bannister, M. T., Lintott, C., et al. 2024, He awa whiria: the tidal streams of interstellar objects, arXiv e-prints, arXiv:2411.14577, doi: [10.48550/arXiv.2411.14577](https://doi.org/10.48550/arXiv.2411.14577)

Francis, P. J. 2005, The Demographics of Long-Period Comets, *ApJ*, 635, 1348, doi: [10.1086/497684](https://doi.org/10.1086/497684)

Fraser, W. C., Pravec, P., Fitzsimmons, A., et al. 2018, The tumbling rotational state of 1I/‘Oumuamua, *Nature Astronomy*, 2, 383, doi: [10.1038/s41550-018-0398-z](https://doi.org/10.1038/s41550-018-0398-z)

Frincke, T. T., Yaginuma, A., Noonan, J. W., et al. 2025, Near-Discovery SOAR Photometry of the Third Interstellar Object: 3I/ATLAS, arXiv e-prints, arXiv:2509.02813, doi: [10.48550/arXiv.2509.02813](https://doi.org/10.48550/arXiv.2509.02813)

Froncisz, M., Brown, P., & Weryk, R. J. 2020, Possible interstellar meteoroids detected by the Canadian Meteor Orbit Radar, *Planet. Space Sci.*, 190, 104980, doi: [10.1016/j.pss.2020.104980](https://doi.org/10.1016/j.pss.2020.104980)

Gaidos, E., Williams, J., & Kraus, A. 2017, Origin of Interstellar Object A/2017 U1 in a Nearby Young Stellar Association?, *RNAAS*, 1, 13, doi: [10.3847/2515-5172/aa9851](https://doi.org/10.3847/2515-5172/aa9851)

Gregg, C. R., & Wiegert, P. A. 2025, A Case Study of Interstellar Material Delivery: alpha Centauri, *The Planetary Science Journal*, 6, 56, doi: [10.3847/PSJ/adb1e9](https://doi.org/10.3847/PSJ/adb1e9)

Grün, E., Landgraf, M., Horányi, M., et al. 2000, Techniques for galactic dust measurements in the heliosphere, *J. Geophys. Res.*, 105, 10403, doi: [10.1029/1999JA900376](https://doi.org/10.1029/1999JA900376)

Grun, E., Zook, H. A., Baguhl, M., et al. 1993, Discovery of Jovian dust streams and interstellar grains by the Ulysses spacecraft, *Nature*, 362, 428, doi: [10.1038/362428a0](https://doi.org/10.1038/362428a0)

Grün, E., Staubach, P., Baguhl, M., et al. 1997, South-North and Radial Traverses through the Interplanetary Dust Cloud, *Icarus*, 129, 270, doi: [10.1006/icar.1997.5789](https://doi.org/10.1006/icar.1997.5789)

Guzik, P., Drahus, M., Rusek, K., et al. 2020, Initial characterization of interstellar comet 2I/Borisov, *Nature Astronomy*, 4, 53, doi: [10.1038/s41550-019-0931-8](https://doi.org/10.1038/s41550-019-0931-8)

Hajduková, Mária, J., & Paulech, T. 2002, in *ESA Special Publication*, Vol. 500, *Asteroids, Comets, and Meteors: ACM 2002*, ed. B. Warmbein, 173–176

Hajduková, M., & Kornoš, L. 2020, The influence of meteor measurement errors on the heliocentric orbits of meteoroids, *Planetary and Space Science*, 190, 104965, doi: [10.1016/j.pss.2020.104965](https://doi.org/10.1016/j.pss.2020.104965)

Hajduková, M., Kornoš, L., & Tóth, J. 2014, Frequency of hyperbolic and interstellar meteoroids, *Meteoritics & Planetary Science*, 49, 63, doi: [10.1111/maps.12119](https://doi.org/10.1111/maps.12119)

Hajduková, M., Sterken, V., Wiegert, P., & Kornoš, L. 2020, The challenge of identifying interstellar meteors, *Planetary and Space Science*, 192, 105060, doi: [10.1016/j.pss.2020.105060](https://doi.org/10.1016/j.pss.2020.105060)

Hajduková, M., Stober, G., Barghini, D., et al. 2024, No evidence for interstellar fireballs in the CNEOS database, *A&A*, 691, A8, doi: [10.1051/0004-6361/202449569](https://doi.org/10.1051/0004-6361/202449569)

Hajduková, Jr., M. 1993, in *Meteoroids and their Parent Bodies*, ed. J. Stohl & I. P. Williams, 61

Hajduková, Jr., M. 1994, On the frequency of interstellar meteoroids., *A&A*, 288, 330

Hajduková, M., Sterken, V., & Wiegert, P. 2019, *Meteoroids: Sources of Meteors on Earth and Beyond* (Cambridge University Press), 235

Hallatt, T., & Wiegert, P. 2020, The Dynamics of Interstellar Asteroids and Comets within the Galaxy: An Assessment of Local Candidate Source Regions for 1I/‘Oumuamua and 2I/Borisov, *AJ*, 159, 147

Hawkes, R. L., Close, T., & Woodwoth, S. 1999, in *Meteoroids 1998*, ed. W. J. Baggaley & V. Porubcan, 257

Hoover, D. J., Seligman, D. Z., & Payne, M. J. 2022, The Population of Interstellar Objects Detectable with the LSST and Accessible for In Situ Rendezvous with Various Mission Designs, *PSJ*, 3, 71, doi: [10.3847/PSJ/ac58fe](https://doi.org/10.3847/PSJ/ac58fe)

Hopkins, M. J., Bannister, M. T., & Lintott, C. 2025a, Predicting Interstellar Object Chemodynamics with Gaia, *AJ*, 169, 78, doi: [10.3847/1538-3881/ad9eb3](https://doi.org/10.3847/1538-3881/ad9eb3)

Hopkins, M. J., Dorsey, R. C., Forbes, J. C., et al. 2025b, From a Different Star: 3I/ATLAS in the context of the Ōtautahi-Oxford interstellar object population model, arXiv e-prints, arXiv:2507.05318, doi: [10.48550/arXiv.2507.05318](https://doi.org/10.48550/arXiv.2507.05318)

Hopkins, M. J., Lintott, C., Bannister, M. T., Mackereth, J. T., & Forbes, J. C. 2023, The Galactic Interstellar Object Population: A Framework for Prediction and Inference, *AJ*, 166, 241, doi: [10.3847/1538-3881/ad03e6](https://doi.org/10.3847/1538-3881/ad03e6)

Hsieh, C.-H., Laughlin, G., & Arce, H. G. 2021, Evidence Suggesting That 'Oumuamua Is the 30 Myr Old Product of a Molecular Cloud, *ApJ*, 917, 20, doi: [10.3847/1538-4357/ac0729](https://doi.org/10.3847/1538-4357/ac0729)

Hui, M.-T., Ye, Q.-Z., Föhring, D., Hung, D., & Tholen, D. J. 2020, Physical Characterization of Interstellar Comet 2I/2019 Q4 (Borisov), *AJ*, 160, 92, doi: [10.3847/1538-3881/ab9df8](https://doi.org/10.3847/1538-3881/ab9df8)

Jacchia, L. G., & Whipple, F. L. 1961, Precision Orbits of 413 Photographic Meteors, *Smithsonian Contributions to Astrophysics*, 4, 97

Jenniskens, P., Baggaley, J., Crumpton, I., et al. 2018, A survey of southern hemisphere meteor showers, *Planetary and Space Science*, 154, 21, doi: [10.1016/j.pss.2018.02.013](https://doi.org/10.1016/j.pss.2018.02.013)

Jewitt, D., Hui, M.-T., Kim, Y., et al. 2020, The Nucleus of Interstellar Comet 2I/Borisov, *ApJL*, 888, L23, doi: [10.3847/2041-8213/ab621b](https://doi.org/10.3847/2041-8213/ab621b)

Jewitt, D., & Luu, J. 2019, Initial Characterization of Interstellar Comet 2I/2019 Q4 (Borisov), *ApJL*, 886, L29, doi: [10.3847/2041-8213/ab530b](https://doi.org/10.3847/2041-8213/ab530b)

Jewitt, D., & Luu, J. 2025, Interstellar Interloper C/2025 N1 is Active, *The Astronomer's Telegram*, 17263, 1

Jewitt, D., Luu, J., Rajagopal, J., et al. 2017, Interstellar Interloper 1I/2017 U1: Observations from the NOT and WIYN Telescopes, *ApJL*, 850, L36, doi: [10.3847/2041-8213/aa9b2f](https://doi.org/10.3847/2041-8213/aa9b2f)

Jewitt, D., & Seligman, D. Z. 2023, The Interstellar Interlopers, *ARA&A*, 61, 197, doi: [10.1146/annurev-astro-071221-054221](https://doi.org/10.1146/annurev-astro-071221-054221)

Kareta, T., Andrews, J., Noonan, J. W., et al. 2020, Carbon Chain Depletion of 2I/Borisov, *ApJL*, 889, L38, doi: [10.3847/2041-8213/ab6a08](https://doi.org/10.3847/2041-8213/ab6a08)

Kareta, T., Champagne, C., McClure, L., et al. 2025, Near-Discovery Observations of Interstellar Comet 3I/ATLAS with the NASA Infrared Telescope Facility, *arXiv e-prints*, arXiv:2507.12234. <https://arxiv.org/abs/2507.12234>

Kim, Y., Jewitt, D., Mutchler, M., et al. 2020, Coma Anisotropy and the Rotation Pole of Interstellar Comet 2I/Borisov, *ApJL*, 895, L34, doi: [10.3847/2041-8213/ab9228](https://doi.org/10.3847/2041-8213/ab9228)

Knight, M. M., Protopapa, S., Kelley, M. S. P., et al. 2017, On the Rotation Period and Shape of the Hyperbolic Asteroid 1I/'Oumuamua (2017 U1) from Its Lightcurve, *ApJL*, 851, L31, doi: [10.3847/2041-8213/aa9d81](https://doi.org/10.3847/2041-8213/aa9d81)

Landgraf, M., Baggaley, W. J., Grün, E., Krüger, H., & Linkert, G. 2000, Aspects of the mass distribution of interstellar dust grains in the solar system from in situ measurements, *J. Geophys. Res.*, 105, 10343, doi: [10.1029/1999JA900359](https://doi.org/10.1029/1999JA900359)

Landgraf, M., & Grün, E. 1998, in IAU Colloq. 166: The Local Bubble and Beyond, ed. D. Breitschwerdt, M. J. Freyberg, & J. Truemper, Vol. 506 (), 381–384, doi: [10.1007/BFb0104750](https://doi.org/10.1007/BFb0104750)

Laughlin, G., & Batygin, K. 2017, On the Consequences of the Detection of an Interstellar Asteroid, *Research Notes of the American Astronomical Society*, 1, 43, doi: [10.3847/2515-5172/aaa02b](https://doi.org/10.3847/2515-5172/aaa02b)

Lecavelier des Etangs, A., Cros, L., Hébrard, G., et al. 2022, Exocomets size distribution in the  $\beta$  Pictoris planetary system, *Scientific Reports*, 12, 5855, doi: [10.1038/s41598-022-09021-2](https://doi.org/10.1038/s41598-022-09021-2)

Levine, W. G., Cabot, S. H. C., Seligman, D., & Laughlin, G. 2021, Constraints on the Occurrence of 'Oumuamua-Like Objects, *ApJ*, 922, 39, doi: [10.3847/1538-4357/ac1fe6](https://doi.org/10.3847/1538-4357/ac1fe6)

Lin, H. W., Lee, C.-H., Gerdes, D. W., et al. 2020, Detection of Diatomic Carbon in 2I/Borisov, *ApJL*, 889, L30, doi: [10.3847/2041-8213/ab6bd9](https://doi.org/10.3847/2041-8213/ab6bd9)

Mamajek, E. 2017, Kinematics of the Interstellar Vagabond 1I/Oumuamua (A/2017 U1), *Research Notes of the American Astronomical Society*, 1, 21, doi: [10.3847/2515-5172/aa9bdc](https://doi.org/10.3847/2515-5172/aa9bdc)

Marčeta, D. 2023, Synthetic population of interstellar objects in the Solar System, *Astronomy and Computing*, 42, 100690, doi: [10.1016/j.ascom.2023.100690](https://doi.org/10.1016/j.ascom.2023.100690)

Marčeta, D., & Seligman, D. Z. 2023, Synthetic Detections of Interstellar Objects with the Rubin Observatory Legacy Survey of Space and Time, *PSJ*, 4, 230, doi: [10.3847/PSJ/ad08c1](https://doi.org/10.3847/PSJ/ad08c1)

Mashchenko, S. 2019, Modelling the light curve of 'Oumuamua: evidence for torque and disc-like shape, *MNRAS*, 489, 3003, doi: [10.1093/mnras/stz2380](https://doi.org/10.1093/mnras/stz2380)

Masiero, J. 2017, Palomar Optical Spectrum of Hyperbolic Near-Earth Object A/2017 U1, *arXiv e-prints*, arXiv:1710.09977. <https://arxiv.org/abs/1710.09977>

Mathews, J. D., Meisel, D. D., Janches, D., Getman, V. S., & Zhou, Q. H. 1999, in *Meteoroids 1998*, ed. W. J. Baggaley & V. Porubcan, 79

McGlynn, T. A., & Chapman, R. D. 1989, On the Nondetection of Extrasolar Comets, *ApJL*, 346, L105, doi: [10.1086/185590](https://doi.org/10.1086/185590)

McKay, A. J., Cochran, A. L., Dello Russo, N., & DiSanti, M. A. 2020, Detection of a Water Tracer in Interstellar Comet 2I/Borisov, *ApJL*, 889, L10, doi: [10.3847/2041-8213/ab64ed](https://doi.org/10.3847/2041-8213/ab64ed)

McNeill, A., Trilling, D. E., & Mommert, M. 2018, Constraints on the Density and Internal Strength of 1I/Oumuamua, *ApJL*, 857, L1, doi: [10.3847/2041-8213/aab9ab](https://doi.org/10.3847/2041-8213/aab9ab)

Meech, K. J., Hainaut, O. R., & Marsden, B. G. 2004, Comet nucleus size distributions from HST and Keck telescopes, *Icarus*, 170, 463, doi: [10.1016/j.icarus.2004.03.014](https://doi.org/10.1016/j.icarus.2004.03.014)

Meech, K. J., Weryk, R., Micheli, M., et al. 2017, A brief visit from a red and extremely elongated interstellar asteroid, *Nature*, 552, 378, doi: [10.1038/nature25020](https://doi.org/10.1038/nature25020)

Meisel, D. D., Janches, D., & Mathews, J. D. 2002a, Extrasolar Micrometeors Radiating from the Vicinity of the Local Interstellar Bubble, *ApJ*, 567, 323, doi: [10.1086/322317](https://doi.org/10.1086/322317)

Meisel, D. D., Janches, D., & Mathews, J. D. 2002b, The Size Distribution of Arecibo Interstellar Particles and Its Implications, *ApJ*, 579, 895, doi: [10.1086/342919](https://doi.org/10.1086/342919)

Micheli, M., Farnocchia, D., Meech, K. J., et al. 2018, Non-gravitational acceleration in the trajectory of 1I/2017 U1 ('Oumuamua), *Nature*, 559, 223, doi: [10.1038/s41586-018-0254-4](https://doi.org/10.1038/s41586-018-0254-4)

Moorhead, A. V., Clements, T. D., & Vida, D. 2020, Realistic gravitational focusing of meteoroid streams, *MNRAS*, 494, 2982, doi: [10.1093/mnras/staa719](https://doi.org/10.1093/mnras/staa719)

Moro-Martín, A. 2022, Interstellar planetesimals, arXiv e-prints, arXiv:2205.04277, doi: [10.48550/arXiv.2205.04277](https://doi.org/10.48550/arXiv.2205.04277)

Moro-Martín, A., & Norman, C. 2022, Interstellar Planetesimals: Potential Seeds for Planet Formation?, *ApJ*, 924, 96, doi: [10.3847/1538-4357/ac32cc](https://doi.org/10.3847/1538-4357/ac32cc)

Moro-Martín, A., Turner, E. L., & Loeb, A. 2009, Will the Large Synoptic Survey Telescope Detect Extra-Solar Planetesimals Entering the Solar System?, *ApJ*, 704, 733, doi: [10.1088/0004-637X/704/1/733](https://doi.org/10.1088/0004-637X/704/1/733)

Musci, R., Weryk, R. J., Brown, P., Campbell-Brown, M. D., & Wiegert, P. A. 2012, An Optical Survey for Millimeter-sized Interstellar Meteoroids, *ApJ*, 745, 161, doi: [10.1088/0004-637X/745/2/161](https://doi.org/10.1088/0004-637X/745/2/161)

Opik, E. J. 1956, Interplanetary Dust and Terrestrial Accretion of Meteoric Matter, *Irish Astronomical Journal*, 4, 84

Opitom, C., Fitzsimmons, A., Jehin, E., et al. 2019, 2I/Borisov: A C<sub>2</sub>-depleted interstellar comet, *A&A*, 631, L8, doi: [10.1051/0004-6361/201936959](https://doi.org/10.1051/0004-6361/201936959)

Opitom, C., Snodgrass, C., Jehin, E., et al. 2025, Snapshot of a new interstellar comet: 3I/ATLAS has a red and featureless spectrum, arXiv e-prints, arXiv:2507.05226, doi: [10.48550/arXiv.2507.05226](https://doi.org/10.48550/arXiv.2507.05226)

Peña-Asensio, E., Trigo-Rodríguez, J. M., & Rimola, A. 2022, Orbital Characterization of Superbolides Observed from Space: Dynamical Association with Near-Earth Objects, Meteoroid Streams, and Identification of Hyperbolic Meteoroids, *AJ*, 164, 76, doi: [10.3847/1538-3881/ac75d2](https://doi.org/10.3847/1538-3881/ac75d2)

Peña-Asensio, E., Visuri, J., Trigo-Rodríguez, J. M., et al. 2024, Oort cloud perturbations as a source of hyperbolic Earth impactors, *Icarus*, 408, 115844, doi: [10.1016/j.icarus.2023.115844](https://doi.org/10.1016/j.icarus.2023.115844)

Peña-Asensio, E., & Seligman, D. Z. 2025, The interstellar flux gap: From dust to kilometer-scale objects, *A&A*, doi: [10.1051/0004-6361/202557337](https://doi.org/10.1051/0004-6361/202557337)

Sekanina, Z. 1976, A Probability of Encounter with Interstellar Comets and the Likelihood of their Existence, *Icarus*, 27, 123, doi: [10.1016/0019-1035\(76\)90189-5](https://doi.org/10.1016/0019-1035(76)90189-5)

Seligman, D., & Laughlin, G. 2018, The Feasibility and Benefits of In Situ Exploration of 'Oumuamua-like Objects, *AJ*, 155, 217, doi: [10.3847/1538-3881/aabd37](https://doi.org/10.3847/1538-3881/aabd37)

Seligman, D. Z., & Moro-Martín, A. 2023, Interstellar objects, *Contemporary Physics*, 63, 200, doi: [10.1080/00107514.2023.2203976](https://doi.org/10.1080/00107514.2023.2203976)

Seligman, D. Z., Farnocchia, D., Micheli, M., et al. 2023, Dark Comets? Unexpectedly Large Nongravitational Accelerations on a Sample of Small Asteroids, *PSJ*, 4, 35, doi: [10.3847/PSJ/acb697](https://doi.org/10.3847/PSJ/acb697)

Seligman, D. Z., Farnocchia, D., Micheli, M., et al. 2024, Two distinct populations of dark comets delineated by orbits and sizes, *Proceedings of the National Academy of Science*, 121, e2406424121, doi: [10.1073/pnas.2406424121](https://doi.org/10.1073/pnas.2406424121)

Seligman, D. Z., Micheli, M., Farnocchia, D., et al. 2025, Discovery and Preliminary Characterization of a Third Interstellar Object: 3I/ATLAS, arXiv e-prints, arXiv:2507.02757, doi: [10.48550/arXiv.2507.02757](https://doi.org/10.48550/arXiv.2507.02757)

Snodgrass, C., Fitzsimmons, A., Lowry, S. C., & Weissman, P. 2011, The size distribution of Jupiter Family comet nuclei, *MNRAS*, 414, 458, doi: [10.1111/j.1365-2966.2011.18406.x](https://doi.org/10.1111/j.1365-2966.2011.18406.x)

Sterken, V. J., Westphal, A. J., Altobelli, N., Malaspina, D., & Postberg, F. 2019, Interstellar Dust in the Solar System, *SSRv*, 215, 43, doi: [10.1007/s11214-019-0607-9](https://doi.org/10.1007/s11214-019-0607-9)

Stern, S. A., Protopapa, S., Freeman, M., et al. 2024, A study of an interstellar object explorer (IOE) mission, *Planet. Space Sci.*, 241, 105850, doi: [10.1016/j.pss.2024.105850](https://doi.org/10.1016/j.pss.2024.105850)

Strub, P., Sterken, V. J., Soja, R., et al. 2019, Heliospheric modulation of the interstellar dust flow on to Earth, *A&A*, 621, A54, doi: [10.1051/0004-6361/201832644](https://doi.org/10.1051/0004-6361/201832644)

Tancredi, G., Fernández, J. A., Rickman, H., & Licandro, J. 2006, Nuclear magnitudes and the size distribution of Jupiter family comets, *Icarus*, 182, 527, doi: [10.1016/j.icarus.2006.01.007](https://doi.org/10.1016/j.icarus.2006.01.007)

Taylor, A. D., Baggaley, W. J., & Steel, D. I. 1996, Discovery of interstellar dust entering the Earth's atmosphere, *Nature*, 380, 323, doi: [10.1038/380323a0](https://doi.org/10.1038/380323a0)

Taylor, A. G., & Seligman, D. Z. 2025, The Kinematic Age of 3I/ATLAS and its Implications for Early Planet Formation, arXiv e-prints, arXiv:2507.08111, <https://arxiv.org/abs/2507.08111>

Trilling, D. E., Robinson, T., Roegge, A., et al. 2017, Implications for Planetary System Formation from Interstellar Object 1I/2017 U1 ('Oumuamua), *ApJL*, 850, L38, doi: [10.3847/2041-8213/aa9989](https://doi.org/10.3847/2041-8213/aa9989)

Trilling, D. E., Mommert, M., Hora, J. L., et al. 2018, Spitzer observations of interstellar object 1I/'Oumuamua, *AJ*, 156, 261

Vaubaillon, J. 2022, Hyperbolic meteors: is CNEOS 2014-01-08 interstellar?, *WGN, Journal of the International Meteor Organization*, 50, 140

Vida, D., Šegon, D., Gural, P. S., et al. 2021, The Global Meteor Network - Methodology and first results, *MNRAS*, 506, 5046, doi: [10.1093/mnras/stab2008](https://doi.org/10.1093/mnras/stab2008)

Von Niessl, G., & Hoffmeister, C. 1925, Katalog der Bestimmungsgrößen für 611 Bahnen Grosser Meteore, *Denkschriften der Kaiserlichen Akademie der Wissenschaften Wien*. Mathematisch-Naturwissenschaftliche Klasse, 100, 1

Štohl, J. 1970, On the problem of hyperbolic meteors, *Bulletin of the Astronomical Institutes of Czechoslovakia*, 21, 10

Weryk, R. J., & Brown, P. 2004, A search for interstellar meteoroids using the Canadian Meteor Orbit Radar (CMOR), *Earth Moon and Planets*, 95, 221, doi: [10.1007/s11038-005-9034-x](https://doi.org/10.1007/s11038-005-9034-x)

Wiegert, P., Tran, V., Gregg, C., Vida, D., & Brown, P. 2025, An Upper Limit on the Interstellar Meteoroid Flux at Video Sizes from the Global Meteor Network, arXiv e-prints, arXiv:2503.19042, <https://arxiv.org/abs/2503.19042>

Wiegert, P. A. 2014, Hyperbolic meteors: Interstellar or generated locally via the gravitational slingshot effect?, *Icarus*, 242, 112, doi: [10.1016/j.icarus.2014.06.031](https://doi.org/10.1016/j.icarus.2014.06.031)

Williams, G. V., Sato, H., Sarnecky, K., et al. 2017, Minor Planets 2017 SN\_33 and 2017 U1, *Central Bureau Electronic Telegrams*, 4450, 1

Xing, Z., Bodewits, D., Noonan, J., & Bannister, M. T. 2020, Water Production Rates and Activity of Interstellar Comet 2I/Borisov, *ApJL*, 893, L48, doi: [10.3847/2041-8213/ab86be](https://doi.org/10.3847/2041-8213/ab86be)

Yang, B., Li, A., Cordiner, M. A., et al. 2021, Compact pebbles and the evolution of volatiles in the interstellar comet 2I/Borisov, *Nature Astronomy*, doi: [10.1038/s41550-021-01336-w](https://doi.org/10.1038/s41550-021-01336-w)

Ye, Q., Kelley, M. S. P., Bolin, B. T., et al. 2020, Pre-discovery Activity of New Interstellar Comet 2I/Borisov beyond 5 au, *AJ*, 159, 77, doi: [10.3847/1538-3881/ab659b](https://doi.org/10.3847/1538-3881/ab659b)

Ye, Q.-Z., Zhang, Q., Kelley, M. S. P., & Brown, P. G. 2017, 1I/2017 U1 ('Oumuamua) is Hot: Imaging, Spectroscopy, and Search of Meteor Activity, *ApJL*, 851, L5, doi: [10.3847/2041-8213/aa9a34](https://doi.org/10.3847/2041-8213/aa9a34)

Zinner, E. 2014, in *Meteorites and Cosmochemical Processes*, ed. A. M. Davis, Vol. 1 (), 181–213